Journal of Thermal Analysis and Calorimetry, Vol. 59 (2000) 187–203

Dedicated to Prof. Edith A. Turi in recognition of her leadership in education

THE PRINCIPLES OF MICRO-THERMAL ANALYSIS AND ITS APPLICATION TO THE STUDY OF MACROMOLECULES

I. Moon, R. Androsch, W. Chen and B. Wunderlich[*]

Department of Chemistry, The University of Tennessee, Knoxville, TN 37996-1600 and Chemical and Analytical Sciences Division, Oak Ridge National Laboratory, Oak Ridge TN 37831-6197 USA

Abstract

A newly developed Micro-Thermal Analyzer affords images based on thermal properties such as thermal conductivity, thermal diffusivity, and permits localized thermal analyses on samples of a square micrometer area by combining the imaging ability of the atomic force microscope and the thermal characterization ability of temperature-modulated differential scanning calorimetry. Since thermal penetration depth depends on frequency, one can obtain depth profiles of thermal conductivity and thermal diffusivity by varying the modulation frequency. Also, the analyzer can be used to characterize phase-transition temperatures, such as glass and melting transitions, of small sample regions with a precision of about ±3 K. Heating rates can be varied between 1 and 1500 K min^{-1}. Modulation frequencies can be applied in the range from 2 to 100 kHz. We applied this new type of instrument to characterize microscopic thermal and structural properties of various polymer systems. The operation principles of the instrument are described, application examples are presented, and the future of the technique is discussed.

Keywords: atomic force microscopy, microcalorimetry, polymers, temperature-modulation

Introduction

Since the inventions of the scanning tunneling microscope [1] (STM) and the atomic force microscope [2] (AFM) which both made revolutionary progress in the field of microscopy, there have been a number of efforts to adapt these atomic scale imaging abilities to scanning thermal microscopy to detect variations of thermal properties and produce images based on these. The first attempt was made by Williams and Wickramasinghe [3] who used the STM. Sub-micrometer spatial resolution was achieved with a thermocouple tip of which the average height from a sample surface was controlled to have a constant *ac* thermal coupling with the surface. Nonnenmacher and Wickramasinghe [4] employed an AFM to obtain thermal conductivity images by measuring the temperature dependence of electrochemical potential differences between tip

* Author to whom all correspondence should be addressed.

1418–2874/2000/ $ 5.00
© 2000 Akadémiai Kiadó, Budapest
Akadémiai Kiadó, Budapest
Kluwer Academic Publishers, Dordrecht

and sample. More recently, Majumdar *et al.* [5] developed a simple measuring technique using a V-shaped thermocouple tip which acts as a temperature sensor as well as the topology sensor of the AFM cantilever by maintaining a constant contact force with the sample surface utilizing the piezoelectric feedback of the AFM. Pylkki *et al.* [6] introduced a Wollaston wire for the same purpose. The Wollaston wire consists of silver of 75 μm diameter, and contains a platinum core about 3 μm in diameter. The core is exposed to make the AFM sensor tip. The platinum tip is then used as a heat source through resistive heating, as well as a resistance thermometer. Finally, Hammiche *et al.* [7, 8] extended this technique by adapting modulation techniques which add the ability to analyze microscopic thermal properties by utilizing the methods of temperature-modulated differential scanning calorimetry (TMDSC) [9]. In 1998 TA Instruments, Inc. developed a commercial Micro-Thermal Analyzer, the μTA™ 2990. The Micro-Thermal Analyzer has at present a 1.0 μm spatial resolution with a Wollaston-wire probe and produces thermal conductivity and thermal diffusivity, as well as topography images. Also, it is possible to carry out localized thermal analysis at a fixed location using the same methods as are available for TMDSC.

Fig. 1 Photograph of the TA Instrument Inc. μTA™ 2990, Micro-Thermal Analyzer (courtesy of TA Instruments)

In this work, we used the commercial μTA™ 2990 to obtain microscopic structure information, thermal images, and localized thermal properties of macromolecules. To anticipate more quantitative analyses through thermal imaging and localized thermal-property measurements, we describe the details of the operation principles of the Micro-Thermal Analyzer. Also, several experimental examples on macromolecules are presented and a general assessment of the technique is given for the future of analysis of macromolecules by micro-thermal analysis.

Instrumentation

The Micro-Thermal Analyzer system by TA instruments is shown in Fig. 1. It consists of a Topometrix Explorer™ AFM which uses thermal probes, as well as conventional AFM topology probes, and control units for piezoelectric and temperature feedback. The figure shows the major piezoelectric assembly in the center, the laser

probe and a video camera for positioning and direct observation of sample and probe on the side, all placed on the cell base, which allows placement and coarse positioning of the sample.

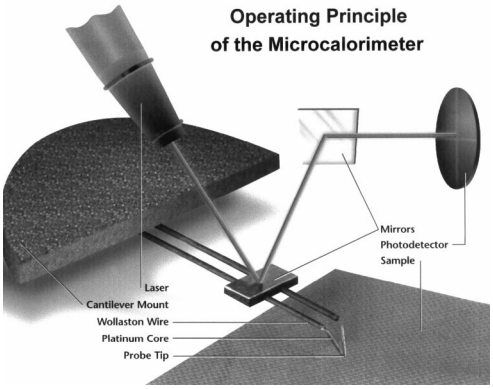

Fig. 2 Schematic of the thermal probe (courtesy of TA Instruments)

Windows NT™-based software serves for the data acquisition and analysis. The cantilever part of the thermal probe is made of a Wollaston wire. The V-shaped tip is shown in Fig. 2. It is made of a 200 μm length platinum-core wire which extends from the silver jacket of the Wollaston wire and is the most resistive part of the probe. By measuring the electrical resistance of the overall Wollaston wire, the average temperature of the platinum-wire tip can be determined. The mirror attached to the cantilever arms serves to reflect the laser beam for the usual, piezoelectric control for the positioning of the platinum tip (Fig. 2).

Operation principles

Local thermal analysis

Figure 3a shows the schematic diagram of a control circuit for the localized thermal analysis. The sample probe contacts the surface at a fixed location with a programmed force, controlled by the piezoelectric feedback. An identical reference probe is attached next to the sample-probe with its tip floating without contact to the sample, allowing for differential measurements. Equal *dc* currents, I, are applied to both probes and are controlled by the temperature-feedback circuit, FB, to achieve a temperature-ramping speed in the range of 1 to 1,500 K min^{-1}. The temperature of the sample probe, T_s, can be determined, after calibration from the resistance of the sample probe, R_s. Since the resistance of platinum has an almost linear dependence on temperature in the range of 300–600 K, R_s, can be expressed by:

$$R_s = R_{s0}[1+\alpha(T_s - T_0)] \quad (1)$$

where R_{s0} and α are the resistance and its temperature coefficient of the platinum wire at room temperature, T_0. The resistance of all lead wires and the Wollaston-portion of the temperature sensor are neglected because of their small resistance when compared to the V-shaped platinum tip. The magnitudes for R_{s0} and α of the platinum tip are about 3 Ω and 0.004 K^{-1}, respectively.

In addition to the *dc* current, an *ac* current can be superimposed on the tip of the μTA™ to obtain a desired temperature-modulation in analogy to the TMDSC operation. The *dc* difference of power between the sample and reference probes is determined by measuring the *dc* voltage difference between two probes after low-pass filtering (LPF) and the *ac* voltage difference is measured by the lock-in amplifier (LIA). This arrangement permits an easy deconvolution of the underlying, *dc* and the reversing *ac* effects.

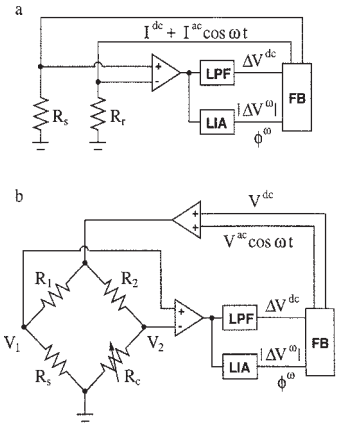

Fig. 3 Schematic of the control circuit for localized thermal analysis (a) and thermal imaging (b). For details and nomenclature see text; *R* are resistances, *I*, currents, *V*, voltages, ϕ phase angles and ω is the modulation frequency

In conventional TMDSC, the total heat capacity is obtained from the *dc* part of the power representing the total heat flow and the average (underlying) heating-rate, in analogy to the standard, not modulated DSC. Reversible heat capacities are obtained from the Fourier analysis of the modulated temperature and the corresponding heat-flow response. In the case of the localized thermal analysis with the μTA™, the heat-transfer condition is not as well defined as in TMDSC since the contact area between tip and sample varies when following the changes in surface topography and the heat losses (and gains) of the sample outside of the contact area are not well controlled. However, phase-transition temperatures of specific sample regions having an area of less than a square micrometer can be assessed qualitatively by monitoring the changes of *dc* power, as well as the amplitude of *ac* voltage difference and its phase lag, all linked to the heat-flow change during the transition. Furthermore, it is possible to carry out thermomechanical analysis by monitoring the change of the tip position due to the softening of surfaces at melting and glass transitions. The μTA™ has

thus a broad range of thermal analysis capabilities based on temperature-modulated DTA and thermomechanical analysis.

Imaging utilizing thermal conductivity and diffusivity

The schematic diagram of the circuitry for thermal imaging is shown in Fig. 3b. The sample probe is connected to a Wheatstone bridge with *dc* and *ac* voltages to be applied. First, let us consider the case of a *dc* voltage input, V^{dc}. The *dc* voltage difference between the two arms of the bridge, ΔV^{dc}, is then determined by the resistance components and the applied *dc* voltage as given by the following equation:

$$\Delta V^{dc} = V_1^{dc} - V_2^{dc} = \frac{R_s^{dc} R_2 - R_c R_1}{(R_s^{dc} + R_1)(R_c + R_2)} V^{dc} \tag{2}$$

where R_s^{dc} is the resistance of the μTA™ probe at temperature, T_s^{dc}. If the variable resistor, R_c, is controlled to produce a nearly zero value of ΔV^{dc}, then R_s^{dc}, and with it the temperature T_s^{dc}, is given by the simple equation:

$$R_s^{dc} = \frac{R_1}{R_2} R_c \tag{3}$$

Furthermore, the *dc* power in the probe needed to raise its temperature to the desired value can be seen from Fig. 3b to be:

$$P_s^{dc} = \frac{(V_1^{dc})^2}{R_s^{dc}} = \frac{(V^{dc})^2 R_s^{dc}}{(R_s^{dc} + R_1)^2} \tag{4}$$

If the tip contacts a sample, two major factors affect the *dc* power to maintain the tip temperature constant. One is the contact area which is determined by the topography of the sample surface and the other is the thermal conductivity of the sample. For example, if we approximate the tip of the μTA™ by a disc with diameter *d* that contacts a semi-infinite medium, the power, P_s^{dc} needed to maintain the average temperature of the heater at T_s^{dc} is given by [10]:

$$P_s^{dc} = \frac{3\pi^2}{8} \kappa d (T_s^{dc} - T_0) \tag{5}$$

where κ is the thermal conductivity of the sample. Therefore, mapping of the power during scanning will contain information about the local thermal conductivity, but will be influenced by changes of the contact area induced by the surface topography.

If an *ac* voltage is applied in addition to the *dc* voltage, to produce a temperature modulation with an angular frequency of ω (=2π/*p* with *p* representing the modulation period), the power across the probe is changed to:

$$P_s(t) = \frac{(V_1^{dc})^2}{R_s^{dc}} \tag{6}$$

$$P_s(t)=\frac{R_s^{dc}}{(R_s^{dc}+R_1)^2}\left[(V^{dc})^2+\frac{(V^{ac})^2}{2}+2V^{dc}V^{ac}\cos\omega t+\frac{(V^{ac})^2}{2}\cos 2\omega t\right] \quad (7)$$

Since the temperature of the probe, T_s, follows the power variation, it is given by:

$$T_s(t)=T_s^{dc}+\left|\delta T_s^{\omega}\right|\cos(\omega t+\varphi_1)+\left|\delta T_s^{2\omega}\right|\cos(2\omega t+\varphi_2), \quad (8)$$

where T_s^{dc} is the temperature determined by the total *dc* power component and expressed by:

$$P_s^{dc} = R_s^{dc}\,[(V^{dc})^2 + (V^{ac})^2/2]/(R_s^{dc} + R_1)^2,$$

and $|\delta T_s^{\omega}|$ and $|\delta T_s^{2\omega}|$ are the amplitudes and φ_1 and φ_2 are the phase-shifts of the first and second harmonic terms, respectively. Also, since according to Eq. (1) the resistance of the probe is linear with temperature, the change of the resistance due to the temperature modulation can be written as follows:

$$R_s(t)=R_s^{dc}+\alpha R_s^{dc}\left|\delta T_s^{\omega}\right|\cos(\omega t+\varphi_1)+\alpha R_s^{dc}\left|\delta T_s^{2\omega}\right|\cos(2\omega t+\varphi_2) \quad (9)$$

and the voltage difference, ΔV, is given by:

$$\Delta V(t)=V_1(t)-V_2(t)=\frac{R_s R_2-R_c R_1}{(R_s+R_1)(R_c+R_2)}(V^{dc}+V^{ac}\cos\omega t) \quad (10)$$

These equations hold since all other components in the Wheatstone bridge are kept at constant temperature. If the temperature dependence of R_s in Eq. (9) is considered, then the *dc* part of ΔV can be approximated by:

$$\Delta V^{dc}\approx\frac{(R_s^{dc}R_2-R_cR_1)V^{dc}+\frac{1}{2}\alpha R_s^{dc}R_2\left|\delta T_s^{\omega}\right|V^{ac}\cos\varphi_1}{(R_s^{dc}+R_1)(R_c+R_2)} \quad (11)$$

Since in the temperature feedback control V^{dc} is usually larger than V^{ac}, and α has a small value, the second term in the numerator of Eq. (11) may be neglected. Therefore, if the bridge-balancing condition of Eq. (3) is maintained by controlling R_c, then the *dc* temperature, T_s^{dc} can be determined from R_c as in the *dc* experiment and ΔV is approximated by the sum of the following three harmonic terms:

$$\Delta V^{\omega}(t)=\frac{\alpha R_s^{dc}R_1}{(R_s^{dc}+R_1)^2}V^{dc}\left|\delta T_s^{\omega}\right|\cos(\omega t+\phi_1)+\frac{1}{2}V^{ac}\left|\delta T_s^{2\omega}\right|\cos(\omega t+\varphi_2) \quad (12)$$

$$\Delta V^{2\omega}(t)=\frac{\alpha R_s^{dc}R_1}{(R_s^{dc}+R_1)^2}\left[\frac{1}{2}V^{ac}\left|\delta T_s^{\omega}\right|\cos(2\omega t+\phi_1)+V^{dc}\left|\delta T_s^{2\omega}\right|\cos(2\omega t+\varphi_2)\right] \quad (13)$$

$$\Delta V^{3\omega}(t)=\frac{\alpha R_s^{dc}R_1}{2(R_s^{dc}+R_1)^2}V^{ac}\left|\delta T_s^{2\omega}\right|\cos(3\omega t+\varphi_2) \quad (14)$$

Being concerned about the quantity which the instrument picks up, V^{dc} is controlled to be an order of magnitude larger than V^{ac}. In this case, the first harmonic signal that is measured by the lock-in amplifier, can be reduced to:

$$\Delta V^{\omega}(t) \approx \frac{\alpha R_s^{dc} R_1}{(R_s^{dc}+R_1)^2} V^{dc} \left|\delta T_s^{\omega}\right| \cos(\omega t+\varphi_1) \tag{15}$$

Equation (15) holds because $|\delta T_s^{\omega}|$ is proportional to the amplitude of the first harmonic of the power $|P_s^{\omega}|$ given by:

$$\left|P_s^{\omega}\right| = \frac{2R_s^{dc} V^{dc} V^{ac}}{(R_s^{dc}+R_1)^2} \tag{16}$$

and $|\delta T_s^{\omega}|$ is also larger than $|\delta T_s^{2\omega}|$ which is proportional to $R_s^{dc}(V^{ac})^2/[2(R_s^{dc}+R_1)^2]$ in Eq. (7). Therefore, the first harmonic amplitude of the temperature modulation $|\delta T^{\omega}|$ can be obtained by measuring the first harmonic amplitude of the voltage difference $|\Delta V^{\omega}|$ in Eq. (15) and it can also be controlled to have a desired value by the feedback control on both of V^{ac} and V^{dc} which determine the power *via* Eq. (16). If under the same condition as assumed for the derivation of Eq. (5) a modulated power $|P_s^{\omega}|$ is supplied to the AFM tip, treated as a disc heater, the average temperature modulation of the disc can be written by [10]:

$$T_s^{\omega}(t) = \frac{8\sqrt{D}}{\pi^{3/2} d^3 \kappa} \int_0^{d/2} r\,dr \int_{-\infty}^{t} dt' \frac{P_s^{\omega}(t')}{\sqrt{t-t'}} \int_0^{\infty} d\lambda \exp[-D(t-t')\lambda^2] J_0(\lambda r) J_1\left(\frac{\lambda d}{2}\right) \tag{17}$$

where thermal diffusivity, D, is defined by $\kappa/(\rho c_p)$ with ρ being the density and c_p the specific heat capacity. Therefore, if $|R_s^{\omega}|$ is controlled and $|P_s^{\omega}|$ is measured, or *vice versa*, one can obtain the information related to thermal conductivity and thermal diffusivity. Also, if the modulation frequency is changed, then the depth profile of the two properties can be obtained because the modulated heat can penetrate only a certain depth from the surface. The thermal penetration depth, λ can be estimated for the modulated heat supplied to the semi-infinite medium by [10]:

$$\lambda = \sqrt{\frac{2D}{\omega}} \tag{18}$$

Since the Micro-Thermal Analyzer measures $|\Delta V^{\omega}|$ to maintain a constant $|T_s^{\omega}|$, the variations of the frequency- or depth-dependent thermal conductivity and thermal diffusivity can be seen in the image mapping of $|\Delta V^{\omega}|$ which is related to $|P_s^{\omega}|$ *via* Eqs (15) and (16). However, ΔV^{dc} in Eq. (15) is also related to the *dc* power, which, in turn, has a close relation to thermal conductivity and *dc* temperature, as shown in the earlier treated *dc* case. Therefore, it must be pointed out that the thermal images obtained from $|\Delta V^{\omega}|$ contain three different pieces of information 1) the frequency- or depth-dependent thermal conductivity and thermal diffusivity, 2) the frequency-independent thermal conductivity, and 3) the surface topography as defined by the contact area d.

Experimental results

Temperature calibration and localized thermal analysis

The thermal probe was calibrated with the melting temperatures of four polymers, poly(oxyethylene) (POE), polypropylene (PP), poly(ethylene terephthalate) (PET), and polytetrafluoroethylene (PTFE). Figure 4 shows as examples the temperature dependencies of the *dc* power and the tip position at the melting temperatures of samples of POE and PET which were also measured using a Mettler-Toledo 820 DSC at the same heating rate of 10 K min^{-1}. In Fig. 5a, the calibration temperatures, measured for each sample at several locations, are shown as a function of resistance of the platinum tip. A linear equation used to fit the data for the specific tip is given in the figure. It can be seen from Fig. 5b that the temperature precision is about ±3 K.

Figure 6 shows an example of the localized thermal analysis performed at a glass transition. Polystyrene was chosen as an example. The result of the *dc* measurement is shown in Fig. 6a. The *dc* power and the tip position show the typical, broad change of the glass transition. In Fig. 6b one can see the changes in the *ac* voltage difference and the phase over the broad temperature range of 353–493 K. To obtain quantitative results from the *ac* measurement, as possible with TMDSC, more work is needed, especially in setting up a proper model for the heat-transfer situation and for the refining the experimental conditions.

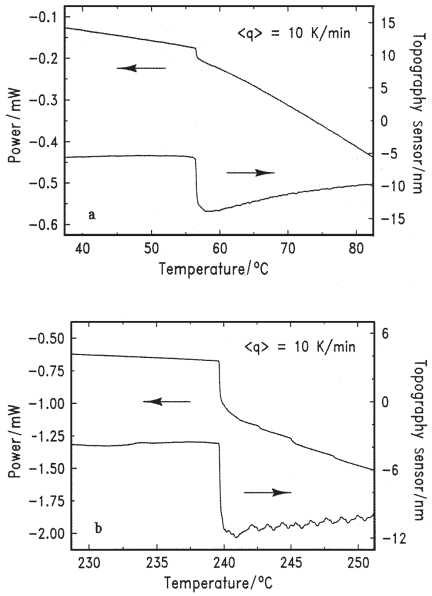

Fig. 4 Local thermal analyses on the melting temperatures of poly(oxyethylene) (a) and poly(ethylene terephthalate) (b). The heating rate <*q*> is 10 K min^{-1}

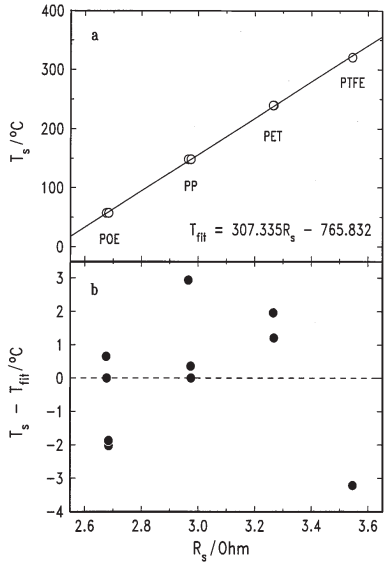

Fig. 5 Calibrated melting temperatures as a function of the tip resistance. The line denotes the fitting result. (b) Plot to estimate the precision of the temperature measurements

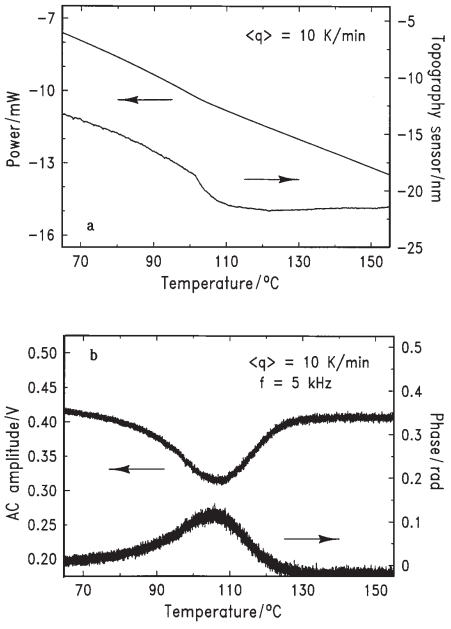

Fig. 6 Local thermal analysis on the glass transition of polystyrene; *dc* measurement (a) and *ac* measurement (b)

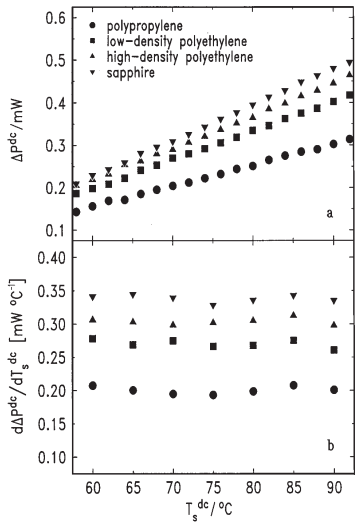

Fig. 7 The *dc* power difference between the sample measurements and the reference measurements of air. (b) The temperature derivatives of the *dc* power difference

Experimental confirmation of the operation principles of thermal imaging

To check the possibility of thermal-conductivity measurements using Eq. (5), P_s^{dc} was measured as a function of T_s^{dc} with about 2 mm thick discs of polypropylene, low-density polyethylene, high-density polyethylene, and sapphire. The measurements were carried out on flat surfaces with identical contact forces to have close to the same contact areas. Figure 7a shows the *dc* power difference, ΔP^{dc} as measured between the sample and air. Since ΔP^{dc} corresponds to P_s^{dc} of Eq. (5) which denotes the net power delivered into the sample, ΔP^{dc} can be substituted for P_s^{dc} in Eq. (5). As expected, ΔP^{dc} shows a linear temperature dependence. Figure 7b displays the temperature derivative, $d\Delta P^{dc}/dT_s^{dc}$, as numerically derived from Fig. 7a. Since these slopes correspond to $3\pi\kappa d/8$ in Eq. (5), they should be proportional to the thermal

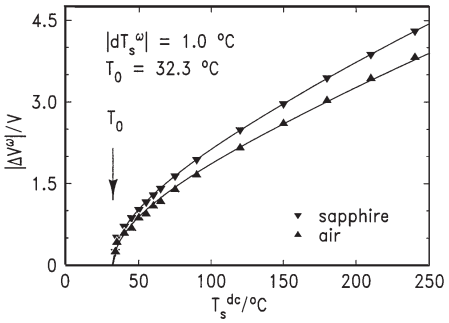

Fig. 8 The amplitude of the first harmonic voltage difference as a function of the tip temperature

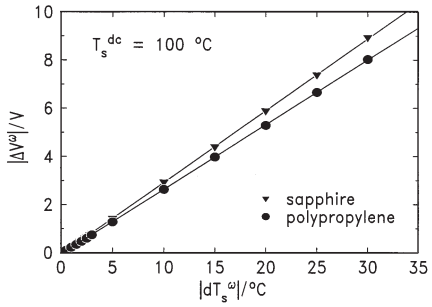

Fig. 9 The amplitude of the first harmonic voltage difference as a function of the first harmonic amplitude of the temperature modulation

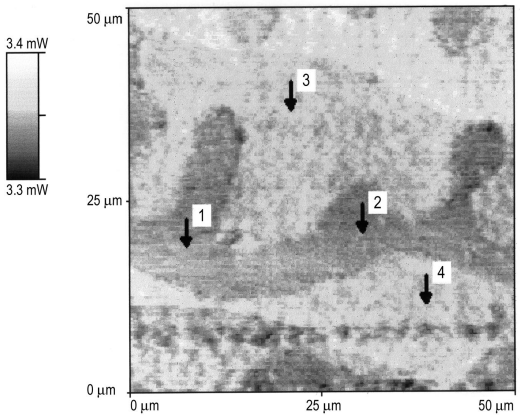

Fig. 10 Thermal conductivity image of a 60/40 PBT/PC blend. The *dc* power is scaled by the color in the left bar and the numbers denote the locations where thermomechanical analyses were carried out

conductivity of the samples if the contact areas are the same, as assumed for Eq. (5). However, the obtained values at room temperature are not proportional to the literature values of thermal conductivity for polypropylene, low density and high density polyethylenes, and sapphire, namely 0.12, 0.33, 0.52 [11], and 33 W m^{-1} K^{-1} [12], respectively. Only the order of the slopes goes parallel to the order of the thermal conductivities, therefore, one may conclude that there are other effects that need to be considered for a quantitative interpretation. Possible effects are, for example, the additional heat flow through the air, the boundary effects due to finite sample dimensions, and a *dc* power dependence of the base temperature, T_0. Also, it should be noticed that the thermal conductivity images obtained from P_s^{dc} do not show real thermal conductivity profiles, but only nonlinearly scaled profiles of thermal conductivity variations. A better image resolution can be obtained when the scanning is per-

formed at higher tip temperatures and when the sample has a lower thermal conductivity because the image resolution is proportional to $d\Delta P^{dc}/d\kappa$.

If the temperature dependences of R_s^{dc} and P_s^{dc} in Eqs (1) and (7) are considered and $V^{ac} \ll V^{dc}$, as is assumed for Eqs (7) and (15), then the temperature dependence of the *ac* voltage difference, $|\Delta V^{\omega}|$ can be expressed by:

$$\left|\Delta V^{\omega}\right| \approx \sqrt{C_1 (T_s^{dc} - T_0)^2 + C_2 (T_s^{dc} - T_0)} \tag{19}$$

where C_1 and C_2 are constants. Figure 8 shows the $|\Delta V^{\omega}|$ data obtained from sapphire and air measurements under the condition of $|\delta T_s^{\omega}|$=1.0 K and $f=\omega/(2\pi)$=8 kHz. The data were fitted to Eq. (19) and the good coincidence between the fitting lines and the measured data is obvious. For this experiment room temperature was measured to be 305.5 K. To check the linear relation between $|\Delta V^{\omega}|$ and $|\delta T_s^{\omega}|$ in Eq. (15), $|\Delta V^{\omega}|$ was measured as a function of $|\delta T_s^{\omega}|$ at a constant T_s^{dc} of 373 K with polypropylene and sapphire. In Fig. 9 one can see the almost perfect linear relations. The slope of the sapphire data is larger than that of the polypropylene data because the slope is proportional to V^{dc} in Eq. (15), and V^{dc} is also proportional to the *dc* power in Eq. (16) which, in turn, is determined by the thermal conductivity. Since $|\delta T_s^{\omega}|$ amplifies $|\Delta V^{\omega}|$ in Eq. (15), a better resolution is obtained in the image by mapping of $|\Delta V^{\omega}|$ if a larger $|\delta T_s^{\omega}|$ is used.

Material characterization in a polymer blend

Figure 10 represents the thermal conductivity image of a 60/40 poly(butylene terephthalate) (PBT) blend with polycarbonate (PC). It can easily be seen that there are two distinct regions which have different thermal conductivity values. The difference between the brighter region in the upper part and the bright region in the middle is due to a topographic height change. To characterize the two different regions, we carried out thermomechanical analysis with a 180 K min^{-1} heating rate at the four different locations marked in Fig. 10. Figure 11 shows the vertical changes of the tip position due to the softening at the glass transition of PC (locations 1 and 2 in Fig. 10)

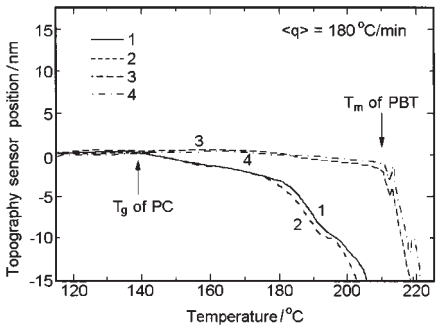

Fig. 11 Thermomechanical analysis on the 60/40 PBT/PC blend. Lines 1 and 2 show the glass transition at around 410 K (140°C) and lines 3 and 4 show the melting temperature of PBT at about 480 K (210°C)

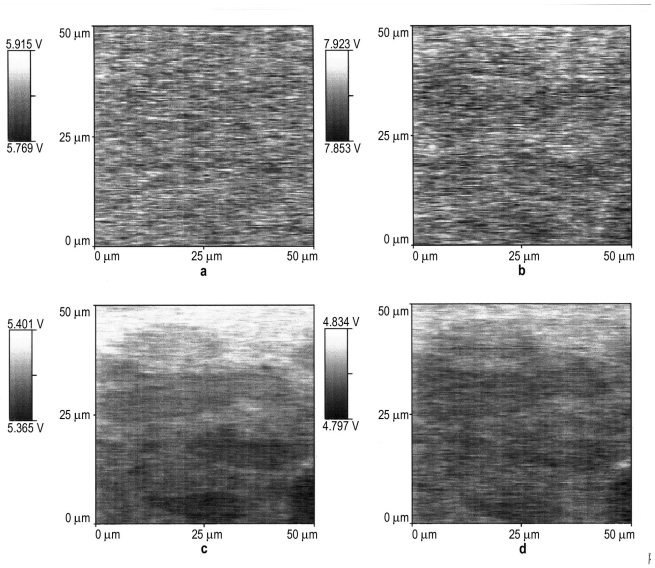

Fig. 12 The images from the first harmonic *ac* voltage difference. The temperature-modulation amplitude is programmed to be 1 (a), 3 (b), 10 K (c) with 2 kHz frequency and 10 K (d) with 64 kHz frequency at 373 K. The absolute voltage values were determined by the amplification conditions of the measurement circuit

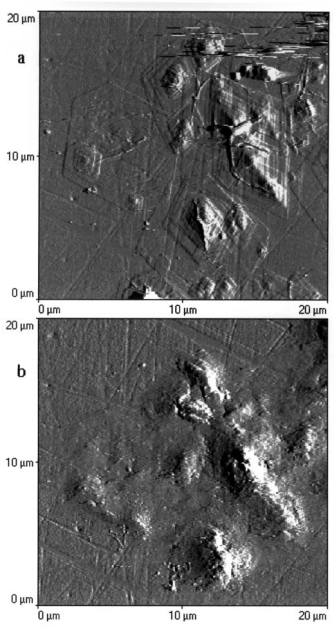

Fig. 13 The AFM image of polyethylene crystals (a). The AFM image of the same structure as (a) after several thermal scans (b)

and the melting transition of PBT (locations 3 and 4). The depth profiles of the two polymer regions were tested with *ac* measurements. First, we found that to achieve a good image resolution, the temperature-modulation amplitude should be larger than 10 K. The dependence of the image resolution on the temperature-modulation amplitude can be seen in Figs 12a, b, and c, which have amplitudes of 1, 3, and 10 K, respectively. The temperature of analysis was 373 K and the modulation frequency, 2 kHz. Figure 12d was obtained with a modulation frequency of 64 kHz at the same temperature. The penetration depth of the modulated heat can be roughly estimated from Eq. (18) to be about 5 μm for 2 kHz and 1 μm for 64 kHz. While there are small differences between Fig. 12c and d, the main domain scheme of the polymers is not changed up to about 5 μm in depth from the surface.

Heating-rate dependence of the melting temperature in polyethylene crystals

Many polymer crystals have a strong heating-rate dependent melting temperature due to a time-dependent structural reorganization before melting [13]. Polyethylene was studied earlier in great detail with results indicating superheating of extended-chain crystals, reorganization of folded-chain lamellae, and zero-entropy-production melting of annealed samples [14]. To make use of the high heating rate capability of the μTA™, we tried to measure the heating-rate dependence in the microscopic sample region and to observe the change of the crystal morphology after delivering heat through a small area to raise the temperature above the melting temperature. These experiments, which may make an important future development, were not fully successful. We found that the thermal tip damages the soft crystal surface even with a minimum contact force for imaging. Figure 13a is a topographic image obtained with a standard Si_3N_4 AFM tip of a sample of solution-grown lamellar polyethylene crystals with a growth-spiral morphology. The polyethylene crystal samples were prepared on a glass substrate by the same method as developed in [15]. The image was shaded by a right-side light for a stereoscopic view. The thickness of a crystal layer is about 15 nm. Figure 13b is the same region as in Fig. 13a, but after several scannings with the thermal tip at room temperature. It can be

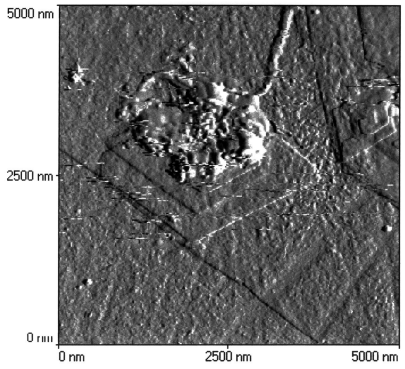

Fig. 14 The AFM image of a melted spot after heating to 407 K at 500 K min^{-1} heating rate

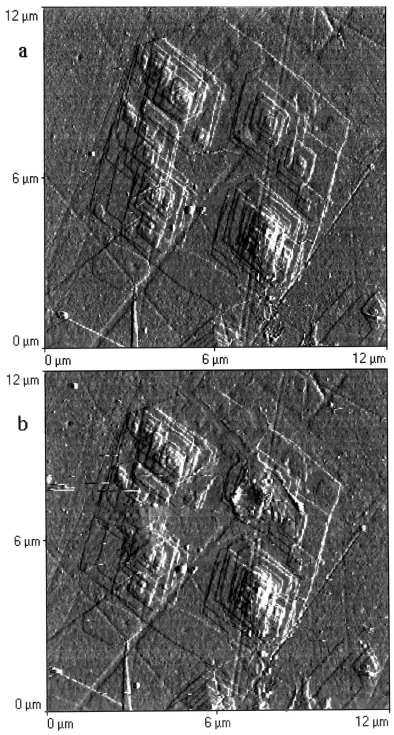

Fig. 15 The AFM image of polyethylene crystals before melting. (b). The location of a large crater is contacted by the thermal tip and heated up to 407 K with a heating rate of 5 K min^{-1}

seen that the crystals are damaged beyond recognition. However, thermomechanical analyses can be performed without thermal scanning by guessing the crystal positions from a reference point on the glass substrate. Figure 14 shows the melted crystal by heating up to 407 K with a heating rate of 500 K min^{-1}. A noticeable change in power and tip position was not found, probably due to the small amount of melting. Figure 15a is a topographic image of a set of crystals before thermomechanical analysis, and Fig. 15b is the image of the same crystals after heating the upper right crystal up to 407 K with a heating rate of 5 K min^{-1}. One can see partially changed crystals also on the left and upper regions of the figure besides the large crater of about 1 μm in diameter on the right crystal. The partially changed structures were probably made by movement of the thermal tip during the thermomechanical analysis. Such movement seems to be induced by vibrational noises and usually occurred in slow measurements at slow heating rates which need a long time to increase the temperature beyond melting. Therefore, a vibration-free condition is needed to perform accurate microscopic thermal analyses on melting transitions of polymers which have rather soft surfaces or which consist of thin layers.

Discussion

We have described the operation principles of the Micro-Thermal Analyzer and checked its abilities for possible applications in the detailed analysis of the areas of interest to the study of the morphology of macromolecules. The analyses already documented in the qualitative application briefs available for the μTA™ could easily be duplicated. Particularly recognition of multi-phase samples with largely different thermal conductivity, such as composites of polymers with, for examples, metals, carbon, or glass of sufficient size. Similarly, the recognition of phase areas by fixed position thermal analysis, as shown in Figs 10 and 11 can be achieved with a precision of about three kelvins, as shown in Figs 4 and 5. These capabilities alone give the microcalorimeter a wide range of applications.

To extend the applicability to the just slightly smaller morphological features of polymer crystals, such as the probing of intercrystalline areas for their glass transition, variability of melting behavior of crystals in different locations, *etc.* improvements are needed. A higher-resolution probe for the thermal analysis, as already in the development stage, is required for better image definition to nanometer-scale resolution. Also, to obtain quantitative thermal information from the thermal scanning and local thermal analysis, new methods need to be developed for temperature sensing and control. For example, if a constant *dc* and an *ac* voltage are programmed and the amplitude of the temperature modulation is measured using Eqs (11) and (15), then one can obtain more accurate depth profiles from scanning because only the temperature modulation contains frequency or depth-dependent information as shown in Eq. (17). Also, the third harmonic signal of Eq. (14), presently not accessible, could be used to measure the thermal properties without a *dc* voltage input, V^{dc}, as has been applied extensively, as described in [16]. In this case, however, a hot stage to control the sample temperature will be needed. Again, a temperature-controlled stage, which would also be of use for other application, is in the development program of TA Instruments for 1999.

These basic new developments supported by the equations derived in this paper should be the foundation for new techniques to change from the present DTA and TMA applications to true calorimetry. Note, that the term DTA is used for describing a differential technique that is quantitative in temperature, but qualitative in calorimetric measurement. The key issues seem to be to develop a tip and measurement technique that allows to handle Eqs (5) and (17) with a constant, predictable value of the contact diameter d and a shorter length of the measured resistance wire for the temperature determination. Next would be the detailed interpretation of phase-angle and *ac*-amplitude, where first data are shown in Fig. 6. As soon as quantitative interpretation is possible, many of the TMDSC applications can be transferred to the microcalorimetry scale. Making use of Eq. (14), it should be possible to use the third harmonic to study reversing phenomena to the many kilohertz region, as is done by the so-called 3ω method. The TMDSC, in contrast, reaches at present only 0.1 Hz. Overall, the microcalorimeter is at the beginning of creating a promising field of polymer analysis not presently covered by any other technique.

This work was supported by the Division of Materials Research, National Science Foundation, Polymers Program, Grant # DMR-9703692 and the Division of Materials Sciences, Office of Basic Energy Sciences, U.S. Department of Energy at Oak Ridge National Laboratory, managed by Lockheed Martin Energy Research Corp. for the U.S. Department of Energy, under contract number DE-AC05-96OR22464. Support by the Korean Research Foundation for the stay of I.M at UTK is gratefully acknowledged. Some support for instrumentation came from TA Instruments, Inc. Figures one and two were provided by TA Instruments. Research support was also given by ICI Paints.

The submitted manuscript has been authored by a contractor of the U.S. Government under the contract No. DE-AC05-96OR22464. Accordingly, the U.S. Government retains a non-exclusive, royalty-free license to publish, or reproduce the published form of this contribution, or allow others to do so, for U.S. Government purposes.

References

1 G. Binnig, H. Rohrer, Ch. Gerber and E. Weidel, Phys. Rev. Lett., 49 (1982) 57.
2 G. Binnig, C. F. Quate and Ch. Gerber, Phys. Rev. Lett., 56 (1986) 930.
3 C. C. Williams and H. K. Wickramasinghe, Appl. Phys. Lett., 49 (1986) 1587.
4 M. Nonnenmacher and H. K. Wickramasinghe, Appl. Phys. Lett., 61 (1992) 168.
5 A. Majumdar, J. P. Carrejo and J. Lei, Appl. Phys. Lett., 62 (1993) 2501.
6 R. J. Pylkki, P. J. Moyer and P. E. West, Jpn. J. Appl. Phys., Part 1 33 (1994) 3785.
7 A. Hammiche, D. J. Hourston, H. M. Pollock, M. Reading and M. Song, J. Vac. Sci. Technol., B14, (1996) 1486.
8 A. Hammiche, M. Reading, H. M. Pollock, M. Song and D. J. Hourston, Rev. Sci. Instrum., 67 (1996) 4268.
9 M. Reading, Trends Polym. Sci., 1 (1993) 248.
10 H. S. Carslaw and J. C. Jaeger, Conduction of Heat in Solids, 2nd Ed., Clarendon Press (Oxford, 1959).
11 Physical Properties of Polymer Handbook, edited by J. E. Mark, American Institute of Physics, Woodbury 1996.
12 CRC Handbook of Chemistry and Physics, 77th Ed., edited by D. R. Lide et al., CRC Press (Boca Raton, 1996).
13 Macromolecular Physics, Volume 3, Crystal Melting, B. Wunderlich. Academic Press, 363 pp., New York, London, (Translated into Russian, MIR, Moscow, 1984), 1980.
14 E. Hellmuth and B. Wunderlich, J. Appl. Phys., 36 (1965) 3039.
15 P. Sullivan and B. Wunderlich, Polymer Letters 2 (1964) 537.
16 I. K. Moon, Y. H. Jeong and S. I. Kwun, Rev. Sci. Instrum., 67 (1996) 29.